

First-principles study of transition metal impurities in Si

Z. Z. Zhang,^{1,2,*} B. Partoens,^{2,†} Kai Chang,^{1,‡} and F. M. Peeters^{2,§}

¹SKLSM, Institute of Semiconductors, Chinese Academy of Sciences, P.O. Box 912, Beijing 100083, People's Republic of China

²Departement Fysica, Universiteit Antwerpen, Groenenborgerlaan 171, B-2020 Antwerpen, Belgium

(Received 25 June 2007; revised manuscript received 25 January 2008; published 2 April 2008)

By using *ab initio* electronic structure calculations within density functional theory, we study the structural, electronic, and magnetic properties of Si doped with a transition metal impurity. We consider the transition metals of the 3*d* series V, Cr, Mn, Fe, Co, and Ni. To get insight into the level filling mechanism and the magnetization saturation, we first investigate the transition metal-Si alloys in the zinc-blende structure. Next, we investigate the doping of bulk Si with a transition metal atom, in which it occupies the substitutional site, the interstitial site with tetrahedral symmetry, and the interstitial site with hexagonal symmetry. It is found that all of these transition metal impurities prefer an interstitial position in Si. Furthermore, we show that it is possible to interpret the electronic and magnetic properties by using a simple level filling picture and a comparison is made to Ge doped with the same transition metal atoms. In order to get insight into the effect of a strained environment, we calculate the formation energy as a function of an applied homogeneous pressure and we show that an applied pressure can stabilize the substitutional position of transition metal impurities in Si. Finally, the energies of the ferromagnetic states are compared to those of the antiferromagnetic states. It is shown that the interstitial site of the Mn dopant helps us to stabilize the nearest neighbor substitutional site to realize the ferromagnetic state. For doping of Si with Cr, a ferrimagnetic behavior is predicted.

DOI: 10.1103/PhysRevB.77.155201

PACS number(s): 75.50.Pp, 71.55.Cn, 71.15.Mb

I. INTRODUCTION

The investigation of transition metal (TM) impurities in semiconductors has received a lot of attention in the last few years due to the enormous potential for applications of room temperature ferromagnetic semiconductors as basic materials for spintronic devices.^{1,2} In particular, much attention has gone to Mn-doped III–V semiconductors, such as GaMnAs and GaMnN, which were thoroughly investigated experimentally and theoretically. Unfortunately, the highest T_c achieved for GaMnAs up to now is 250 K.³ Although T_c of GaMnN is above room temperature, it is well known that *p*-type doping in nitides is very difficult.⁴

More recently, Mn-doped group IV semiconductors also attracted a lot of attention because of their relevance in the present device technology. Most of the experimental⁵ and theoretical^{6,7} attention has gone to Mn-doped Ge. However, adding functionality to the most common semiconductor Si is still in its infancy. Lately, the first reports appeared about room temperature ferromagnetism in Mn-doped Si.⁸ The main difference between Mn-doped Ge and Si is that the Mn atom locates a substitutional site in Ge but an interstitial site in Si. Because a substitutional impurity cannot diffuse as easily as an interstitial one, it may be problematic to reach large enough impurity concentrations in Si before they diffuse into clusters. This motivated the authors of Refs. 9–11 to investigate mechanisms on how the substitutional Mn impurities in Si could be stabilized. Recently, Qian *et al.*¹² proposed a half-metallic digital ferromagnetic heterostructure composed of a δ -doped layer of Mn in Si. A stable Si-based heterostructure with interstitial doped Mn was also proposed.¹³ Experimentally, enhanced room temperature ferromagnetism was found in silicon implanted by Co and Mn.^{14,15}

Concerning Si, most of the interest has been so far limited to doping with Mn. Only a few theoretical works have considered doping with other TM atoms. Pioneering first-

principles Green's-function simulations were performed for isolated impurities in Si.^{16,17} In Ref. 18, Cr and Fe doped Si were considered, however, only in the substitutional configuration. Reference 19 focused on the diffusion of all 3*d* TM atoms in bulk Si, but no spin effects were taken into account in the *ab initio* calculations. Because a careful theoretical study focused on the interaction between TM atoms in a Si matrix, which is based on large supercell density functional calculations that include structural relaxation, is still lacking, we present a systematic study of the TM impurities V, Cr, Mn, Fe, Co, and Ni in Si, as was recently done also for Ge.⁷ In this work, we initially examine if all TMs in Si prefer interstitial doping over substitutional doping and if the tetrahedral or hexagonal interstitial position is favored. Furthermore, the electronic, structural, and magnetic properties for the different TMs in Si are investigated. To get an insight into the effects of strain, we calculate next the formation energies in the case of an applied homogeneous pressure. The energetics of the ferromagnetic state is also compared to the antiferromagnetic ordering. In this work, we want to stress that we focus on neutral TM impurity states. The calculation of the formation energies under *p*-type or *n*-type conditions, as was done for Mn dimers in Si in Ref. 9, is left for future work.

Before discussing the case of isolated TM dopants in Si, we deal with the TM-Si alloy in the zinc-blende structure. Although this structure is not the ground state for these crystals, it is instructive to get insight into its energetics and magnetic properties, which will help us to interpret the results for TM-doped Si.

The present paper is organized as follows: In Sec. II, the computational details are given. The results on the TM-Si alloy are discussed in Sec. III, followed by the results on the isolated dopants in Sec. IV. The effect of a homogeneous applied pressure on these structures is considered in Sec. V. The ferromagnetic and antiferromagnetic orders of these TM atoms in Si are studied by considering several configurations

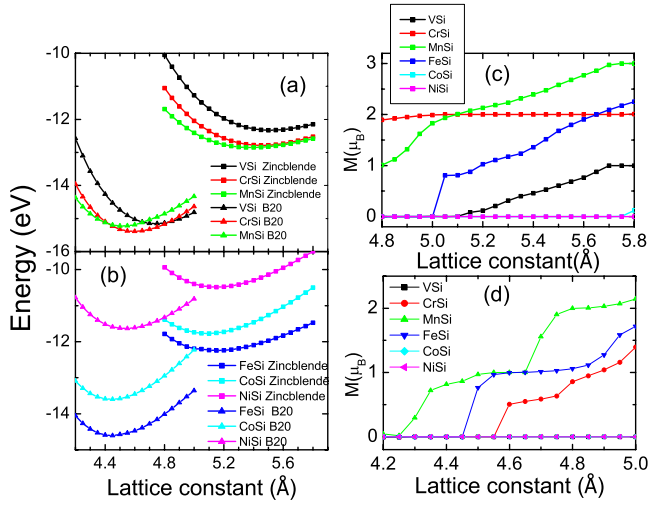


FIG. 1. (Color online) The total energy as a function of the lattice constant for the zinc-blende and B20 crystals of (a) VSi, CrSi, and MnSi and (b) FeSi, CoSi, and NiSi. (c) and (d) show the corresponding magnetic moments for the zinc-blende and B20 structures, respectively.

with different distances between two TM atoms in Sec. VI. Finally, our conclusions are summarized in Sec. VII.

II. COMPUTATIONAL METHOD

The calculations were performed by using the VASP package²⁰ within the generalized gradient approximation (GGA) to density functional theory. We used the projector augmented wave method²¹ and a plane-wave expansion of up to 350 eV for all materials. This results in an accuracy that is better than 1 meV per transition metal atom for the energy difference between the ferromagnetic and antiferromagnetic states. A Perdew-91 functional form²² for the GGA was used.

For the TM-Si alloy calculations, a Monkhorst-Pack k -point sampling of $6 \times 6 \times 6$ was used. Furthermore, we considered low TM concentrations (3%) in Si that corresponded to unit cells containing 32 (one impurity) and 64 (two impurities) atoms. Good convergence was obtained for a Monkhorst-Pack k -point sampling of $4 \times 4 \times 8$ and $4 \times 4 \times 4$ for the supercells with 32 and 64 atoms, respectively. All structures were relaxed until all force components were smaller than 0.01 eV/\AA .

III. TRANSITION METAL IMPURITIES IN Si: ZINC-BLENDE STRUCTURE

As mentioned before, although the TM-Si alloy in the zinc-blende structure is not the ground state crystal structure, it is instructive to look at its electronic and magnetic properties as a function of the lattice constant. It will help us to understand the properties of the isolated TM dopant in Si. Figure 1 shows the energy and the magnetization for the six considered TM-Si structures as a function of the lattice constant. It also shows the energies for the six TM-Si structures in the B20 structure²³ as a function of the lattice constant. It shows that the B20 structure indeed has a lower energy for

TABLE I. The predicted equilibrium lattice constants (a_{calc}), the experimental lattice constants (a_{expt}), and magnetic moments per formula unit (M) for the zinc-blende and B20 structures.

Structure	XSi	a_{calc} (\AA)	a_{expt} (\AA)	M (μ_B)
Zinc blende	VSi	5.518		0.63
	CrSi	5.456		2.0
	MnSi	5.387		2.37
	FeSi	5.158		0.91
	CoSi	5.085		0.0
	NiSi	5.430		0.0
B20	VSi	4.739		0.0
	CrSi	4.600	4.629 ^a	0.51
	MnSi	4.519	4.558 ^a	0.87
	FeSi	4.448	4.489 ^a	0.0
	CoSi	4.442	4.447 ^a	0.0
	NiSi	4.535	4.437 ^a	0.0

^aReference 24.

all considered systems and it is known that it is the ground state structure for CrSi, MnSi, FeSi, CoSi, and NiSi.²⁴ Previous *ab initio* studies of the B20 structure of FeSi and MnSi can be found in literature.²⁵ Table I shows our calculated results and some experimental results of the equilibrium lattice constant, and we find that our predicted values are very close to the experimental values for CrSi up to NiSi for the B20 structure. However, this B20 phase has a Curie temperature of around 30 K only (Ref. 26) and cannot readily account for the high Curie temperature of the materials. In the following, we will concentrate on the results for the zinc-blende structures.

From Fig. 1(c), one can clearly see how the magnetization of VSi, CrSi, and MnSi reaches saturation with increase in the lattice constant. It is remarkable that the magnetic moment of CrSi is already saturated at the equilibrium lattice constant and it almost does not change with the lattice constant. For FeSi, CoSi, and NiSi, it is not clear at which lattice constant the magnetization saturates. We also calculated the density of states (DOS) for these structures at the equilibrium lattice constant, as shown in Fig. 2.

These saturation values and DOS results can be easily understood from a simplified electron filling scheme. The electrons that should be considered are the d and s electrons of the TM and the p electrons from Si. This makes seven electrons for VSi and up to 12 electrons for NiSi. Tetrahedral symmetry splits the fivefold degenerate TM d levels into a threefold degenerate t_2 level and a twofold degenerate e level. The d derived t_2 states strongly couple with the p levels of Si because they have the same symmetry, forming threefold degenerate t_2^b bonding levels and t_2^a antibonding levels, while the e states remain more or less unperturbed, forming nonbonding states that are well localized in energy and space. In Fig. 2, not only the total density of states but also the contribution from the d states is given, which is further split into t_2 and e contributions. The final state and magnetization are now determined by the alignment of ma-

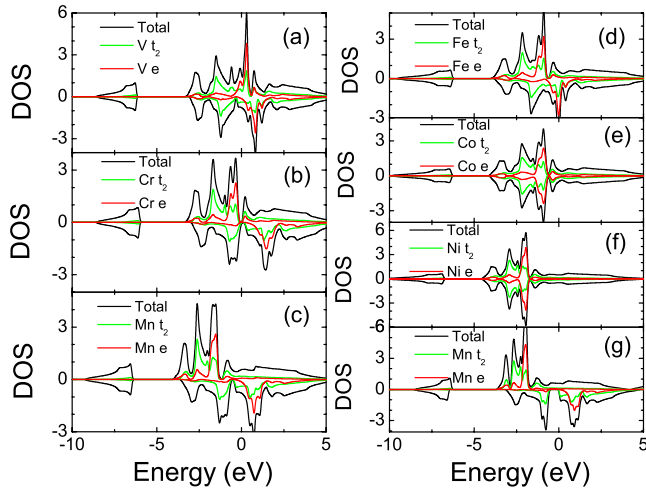


FIG. 2. (Color online) (a)–(f) The DOS for the zinc-blende TM-Si alloys at their equilibrium constant. For each TM-Si alloy, the total DOS is given, together with the contribution to the DOS of the d levels resolved into t_2 and e components. (g) The DOS for the zinc-blende MnSi alloy at the lattice parameter $a=5.75$ Å. The zero of the energy scale is set at the Fermi level.

majority and minority spin levels, which depends on the following: (i) the exchange splitting, which favors parallel spin alignment up to half-filling, (ii) the crystal field splitting, and (iii) the amount of splitting between the bonding and antibonding t_2 levels, i.e., the strength of the p - d coupling. In Fig. 3, this simplified scheme of the levels is shown. The levels under (a) correspond to the unsplit single particle levels. The exchange splitting is taken into account under (b), while the effect of the crystal field splitting is included under (c). In substitutional geometry, it is known that the energy of the e level is below the energy of the t_2 level. The resulting majority and minority levels, including the effect of the p - d coupling, are given under (d) and (e), respectively.

Let us now start filling the levels. Figure 3 schematically shows the two kinds of filling scenarios: one with a strong exchange splitting (upper figure for VSi) and the other with a weak exchange splitting (lower figure for FeSi), and is in comparison to the strength of splitting due to the p - d coupling. In the strong exchange splitting scenario, the minority e level is empty and a high spin state is realized. For such a high spin state, the highest occupied levels are the majority e levels in VSi and CrSi. CrSi corresponds to a closed shell configuration for the majority as well as for the minority levels, which is the reason why the magnetization does not change much if the lattice constant is varied around its ground state value. From the DOS results for CrSi [see Fig. 2(b)], one can indeed also see that a small gap exists at the Fermi energy for both the majority and minority spin states. For MnSi, the maximum magnetization would be reached if the highest occupied energy level were the antibonding t_2^a majority level, leading to a magnetization of $3\mu_B$. The actual value is less as the e minority level is also partly occupied. The magnetization increases with increasing lattice parameter as this diminishes the p - d level coupling. Consequently, the antibonding t_2^a goes down in energy, and the electron completely occupies this majority spin level. This scenario is

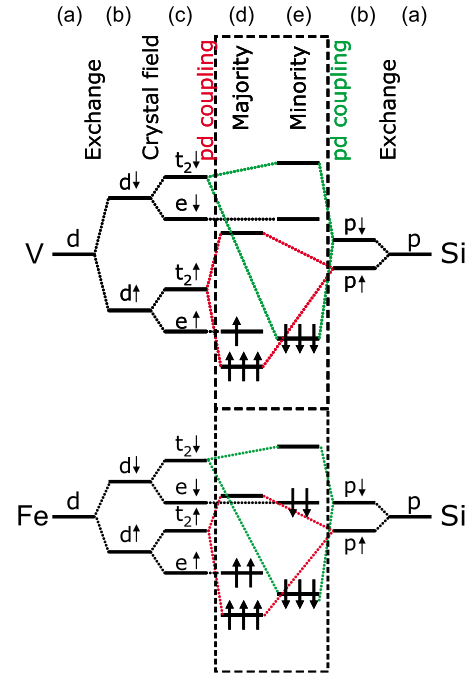


FIG. 3. (Color online) Simplified level filling schemes for the zinc-blende TM-Si alloys for the two different conditions. The first is the high-spin state for VSi and the second is the low-spin state for FeSi. (a) The unsplit single particle levels, (b) the levels with the exchange splitting included, (c) the effect of the crystal field splitting, (d) the resulting majority levels, and (e) the resulting minority levels due to the p - d coupling.

confirmed by the DOS of MnSi shown in Fig. 2(g), calculated for a lattice parameter of $a=5.75$ Å, which is almost 6% larger than the equilibrium lattice parameter. In this situation, MnSi exhibits the half-metal property. If we assume that the minority e level is empty due to a strong exchange splitting, the high-spin state is realized. This single particle picture also predicts the maximum magnetic moment for FeSi and CoSi to be $4\mu_B$ and $5\mu_B$, respectively, when two and three electrons occupy the majority t_2^a antibonding level. The extra electron in NiSi can go only to the minority e level, leading to a maximum magnetic moment of $4\mu_B$. These values are not at all reached around the equilibrium value for the lattice constant because the minority e levels are also occupied. If we assume that the minority e levels are fully occupied, which corresponds to the weak splitting scenario, the low spin state is realized. In this scenario, the magnetic moments for FeSi, CoSi, and NiSi are $0\mu_B$, $1\mu_B$, and $0\mu_B$.

IV. ISOLATED DOPANTS IN Si

We considered TM concentrations of around 3%, which correspond to unit cells with 32 atoms. The size of the unit cell was taken fixed; the atomic positions within the cell were fully relaxed. The TM dopant can be localized in different positions. We considered the substitutional site (replacing one Si atom in the diamond lattice by a TM atom) and two interstitial sites of the diamond lattice, i.e., one tet-

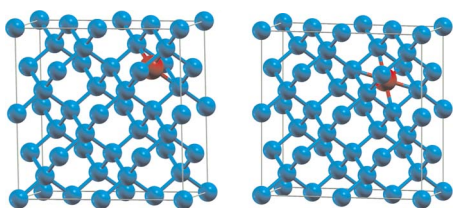


FIG. 4. (Color online) The two considered interstitial positions: one with tetrahedral T_d symmetry (left panel) and one with hexagonal D_{3d} symmetry (right panel). The small blue atoms are Si atoms and the big gray atom is the TM atom.

rahedrally coordinated and one with hexagonal symmetry, as indicated in Fig. 4. For all these positions, the formation energy was calculated. The formation energy is defined as the energy needed to insert a TM atom (taken from a reservoir) into the bulk Si crystal after removing one Si atom in the case of substitutional doping (to a reservoir, taken as bulk Si),

$$E_f = E(\text{Si with TM dopant}) - E(\text{bulk Si}) - \mu_{\text{TM}} + n\mu_{\text{Si}}, \quad (1)$$

with $n=1$ for substitutional doping and $n=0$ for interstitial doping, μ_{Si} as the chemical potential of Si (here, set equal to the total energy per atom of bulk Si), and μ_{TM} as the chemical potential of the TM atom. The choice of the reservoir that provides the species to form the impurity is, unfortunately, a delicate issue. However, we make the same choice as was recently done in the study of TM impurities in Ge,⁷ i.e., the energy per atom of nonmagnetic bcc V, antiferromagnetic bcc Cr, antiferromagnetic fcc Mn, ferromagnetic bcc Fe, ferromagnetic hcp Co, and ferromagnetic fcc Ni. Figure 5(a) shows the formation energy for the different TM impurities in Si. From these results, we see that the tetrahedral interstitial site is favored for all TM atoms except for Ni, in which case the hexagonal interstitial site is the ground state.

It is interesting to compare these results to the corresponding case for Ge, as given in Fig. 6. The results for the

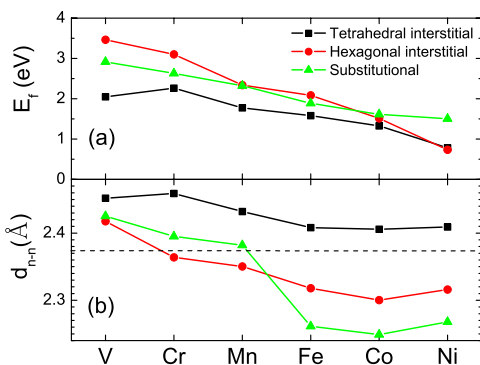


FIG. 5. (Color online) (a) The formation energies for the doping of Si with a TM atom at the substitutional site, the interstitial site with tetrahedral symmetry, and the interstitial site with hexagonal symmetry for the different TM atoms. (b) The nearest neighbor distances between a TM atom and Si for the different doping positions for the different TM atoms.

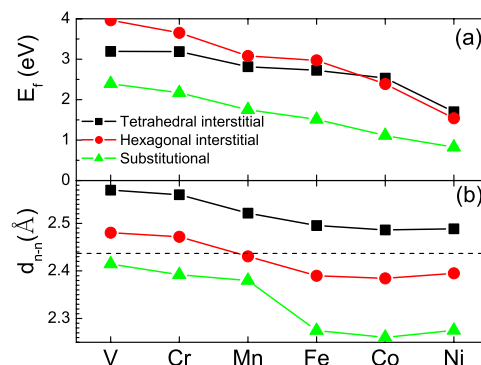


FIG. 6. (Color online) The same as Fig. 5 but for doping of Ge.

substitutional and tetrahedral doping sites agree with those in Ref. 7. It is clear that the TM dopants in Ge always prefer the substitutional site. However, note that the hexagonal interstitial site is preferred over the tetrahedral interstitial site for Co and Ni, which was not considered in Ref. 7.

In Fig. 5(b), the relaxed TM-Si distances for the three doping positions are given. The tetrahedral interstitial always leads to a bond length that is larger than the ideal Si-Si bond length. The TM-Si bond length for a TM atom at a hexagonal interstitial site is, of course, smaller than for the TM atom at the tetrahedral interstitial site. The behavior for the TM atom at the substitutional site is rather surprising; for V, Cr, and Mn, the distance between the TM atom and Si is larger than the ideal Si-Si bond length, while for Fe, Co, and Ni, this distance suddenly drops, leading to a contraction with respect to the Si-Si bond length. This differs from the situation of substitutional doping of TM atoms in Ge [see Fig. 6(b)], in which case a more uniform behavior and a contraction were always found⁷ [see also Fig. 6(b)].

We just showed that in Si all TM atoms will occupy an interstitial site, while in Ge they will occupy a substitutional site. However, note that the energy difference between the lowest interstitial site and the substitutional site for the TM atom in Si is between 0.3 eV (for Fe and Co) and 0.9 eV (for V), while the energy difference between the substitutional site and the lowest interstitial site for the TM atom in Ge is between 0.7 eV (for Ni) and 1.3 eV (for Co). Therefore, we can expect relatively more occupied substitutional sites in Si than interstitial ones in Ge. Let us now consider the electronic and magnetic properties of the interstitial dopants. Figure 7 shows the calculated total magnetic moments for the different TMs in Si and for the three different positions of the dopant. In Fig. 8, the corresponding density of states is given. We can again understand these results from a simplified level filling scheme. The situation for TM impurities at interstitial sites is different from those at substitutional sites (which are similar as for the alloys discussed before). The tetrahedral interstitial site has the same symmetry as the substitutional site and, therefore, the d levels are still split into a doublet e level and a triplet t_2 level. However, in contrast to the substitutional site, now, the energy of the t_2 level is below the energy of the e level, as can also be seen in the density of states plots in Fig. 8. For the hexagonal interstitial site, the t_2 triplet is further split into a singlet and a doublet. The tetra-

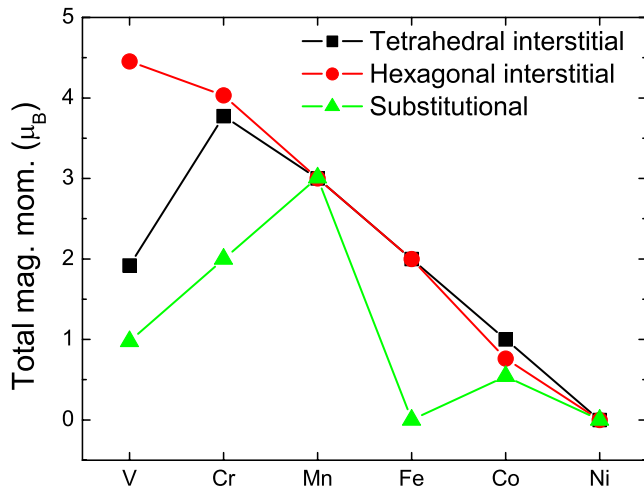


FIG. 7. (Color online) Total magnetic moments for a TM atom doped in Si at a substitutional site, an interstitial site with tetrahedral symmetry, and an interstitial site with hexagonal symmetry.

hedral and the hexagonal interstitial sites have no Si p orbitals pointing to them. Consequently, there is also much less mixing between the p orbitals of Si and the d orbitals of the interstitial TM impurity. Thus, only the d levels of the TM atom are involved in our simplified level filling picture. This makes five electrons for V and up to ten electrons for Ni. As a result, we expect magnetic moments of $5\mu_B$, $4\mu_B$, and $3\mu_B$ for V, Cr, and Mn, respectively, while for the more than half-filled case, we expect $2\mu_B$, $1\mu_B$, and $0\mu_B$. As can be seen from Fig. 7, these predictions are well reproduced by our calculations. The magnetization for doping with V at the hexagonal interstitial only slightly differs from our prediction due to the extent of the d energy level and the small occupation of the t_2 minority level. However, the magnetization for V at the tetrahedral interstitial position strongly differs from our prediction because the exchange splitting is found to be smaller than the crystal field splitting. As can be seen from the projected DOS plot for V in Fig. 8(a), the Fermi energy also cuts the t_2 minority level. The exchange splitting is not large enough to reach full polarization.

The electronic and magnetic properties of the substitutional site can be understood from the same simplified level filling picture that we used to understand the alloy case. The high-spin state is found for V, Cr, and Mn. From the DOS for Si substitutionally doped with Mn [see Fig. 8(j)], it can be seen that not only is the majority antibonding t_2^a level lower in energy than the minority e level but also the minority e level is quite close to the Fermi energy. Therefore, in the case of substitutional doping with Fe, two electrons move to the minority e level, leaving the majority antibonding level t_2^a unoccupied (see the low spin state in Fig. 3). This results in a state with an equal number of majority and minority occupied states, thus driving the system into a nonmagnetic state, as confirmed by the DOS for Si substitutionally doped with Fe [see Fig. 8(m)]. However, Co has again a magnetic moment of $1\mu_B$, with one electron in the majority antibonding t_2^a level. The ferromagnetic Si substitutionally doped with Ni is not stable anymore and becomes nonmagnetic.

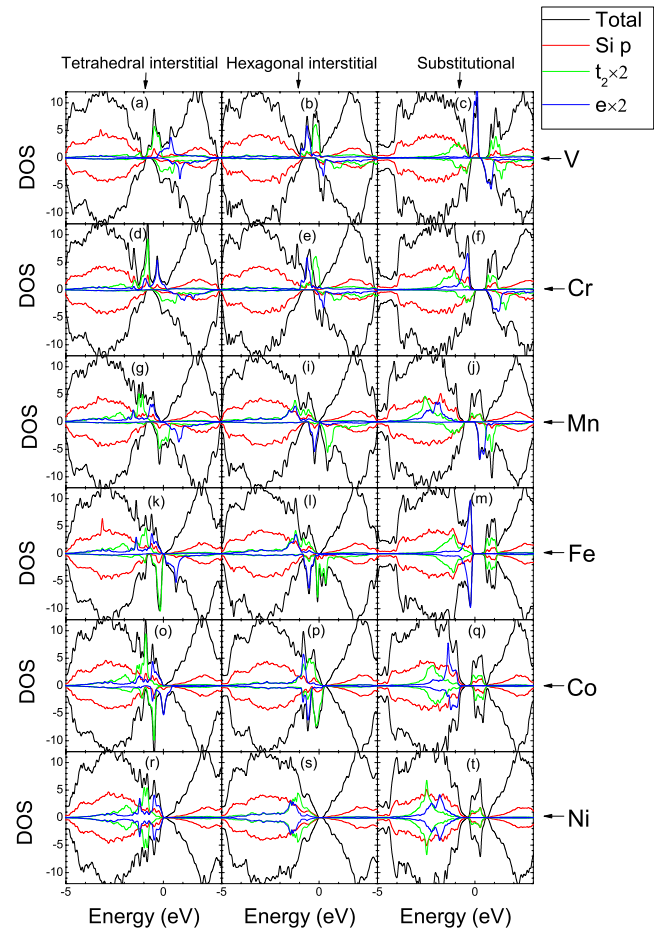


FIG. 8. (Color online) The DOS for the TM atoms doped in Si at a substitutional site, an interstitial site with tetrahedral symmetry, and an interstitial site with hexagonal symmetry. For each TM atom, the total DOS is given, together with the contribution to the DOS of the d levels, which are resolved into t_2 and e components, and the contribution of the Si p levels. The zero of the energy scale is set at the Fermi level.

V. ISOLATED DOPANTS IN STRAINED SI

As shown above, all TM impurities prefer an interstitial site in Si under equilibrium circumstances. However, strain fields can be present in bulk Si crystals, which can be caused by grain boundaries, or induced by the presence of self-assembled Ge dots in the Si matrix, or even by an applied hydrostatic pressure. In order to get some insight into what can be the effect of such strain fields on the studied impurities, we investigate the effect of a homogeneous applied pressure. In Fig. 9, we show the formation energies for the tetrahedral interstitial, hexagonal interstitial, and substitutional positions for the six studied TM impurities in Si as a function of the lattice constant. The needed pressure to realize the change in lattice constant is shown in Fig. 10, which is obtained from a fit of the energy of bulk Si as a function of its volume to Murnaghan's equation. Note that by applying a positive pressure, the substitutional site can be favored for Mn, Fe, Co, and Ni in Si. Of course, applying a pressure also changes the total magnetic moment. The evolution of the total magnetic moment as a function of the lattice parameter

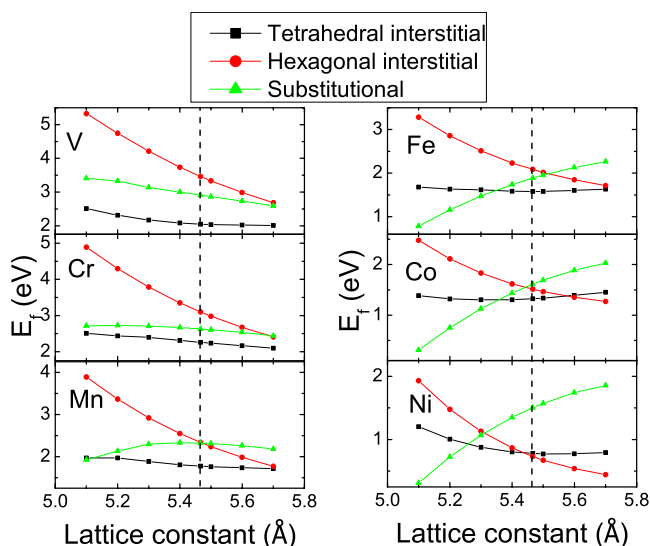


FIG. 9. (Color online) The formation energies for the doping of Si with a TM atom as a function of the lattice constant for the different TM atoms at the substitutional site, the interstitial site with tetrahedral symmetry, and the interstitial site with hexagonal symmetry. The dashed lines correspond to the results for the equilibrium lattice constant.

for all transition metals and the three considered positions is shown in Fig. 11. Just as for the TM alloys, we find that the total magnetic moment decreases with decreasing lattice constant. For the lattice constant at which Mn prefers the substitutional position, its total magnetic moment is decreased to $1\mu_B$.

VI. FERROMAGNETIC, ANTIFERROMAGNETIC, AND FERRIMAGNETIC ORDERINGS

Finally, to analyze the magnetic order, we study the ferromagnetic and antiferromagnetic orderings of two TMs in a $2 \times 2 \times 2 a^3$ supercell (where a is the lattice constant of silicon), which corresponds to TM concentrations of about 3%. The size of the unit cell was taken fixed; the atomic positions within the cell were fully relaxed. We consider three different

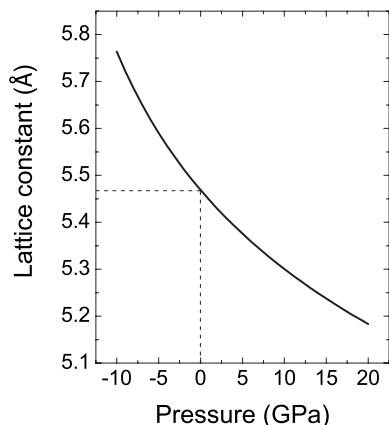


FIG. 10. The lattice constant of bulk Si as a function of the applied homogeneous pressure.

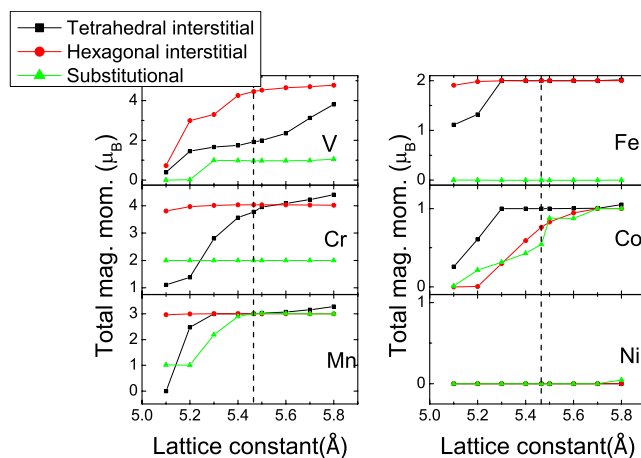


FIG. 11. (Color online) The total magnetic moments as a function of the lattice constant for a TM atom doped in Si at a substitutional site, an interstitial site with tetrahedral symmetry, and an interstitial site with hexagonal symmetry. The dashed lines correspond to the results for the equilibrium lattice constant.

situations: (i) the two TMs are at substitutional sites ($X_S X_S$), where X denotes a TM atom, (ii) two TMs are at tetrahedral interstitial sites ($X_T X_T$), and (iii) one TM is at a substitutional site and the other is at a tetrahedral interstitial site ($X_S X_T$). For the first situation, we consider nine configurations depending on the distance between the two TMs. Each configuration can be labeled by three numbers to represent the (x, y, z) coordinates in units of $a/4$ (as was also done in Ref. 6), while the other TM atom is at $(0, 0, 0)$. The nine configurations are, respectively, N_{111} , N_{220} , $N_{11\bar{3}}$, N_{400} , N_{331} , N_{224} , $N_{33\bar{3}}$, N_{440} , and N_{444} , where $\bar{3}$ denotes -3 . The configurations in the second situation are the same except that the TMs are at the tetrahedral interstitial sites. In the third situation, there are only eight configurations, which are $N_{\bar{1}\bar{1}\bar{1}}$, N_{200} , $N_{\bar{1}\bar{1}\bar{3}}$, N_{222} , $N_{\bar{1}33}$, N_{240} , N_{333} , and N_{244} .

Our results for Si doped with Mn are summarized in Table II. It shows the formation energy per Mn atom for all considered configurations in the three situations, together with the energy difference between the ferromagnetic (FM) and antiferromagnetic (AFM) orderings. It also shows the distance between both TM atoms, before and after the relaxation, and the total magnetic moments for the FM and AFM states.

For the Mn_5Mn_5 situation, we find that the ground state is of configuration N_{111} , which is AFM. When the distance (d_{Mn-Mn}) between the Mn impurities increases, we find that the FM state is always favored. The results for the ground state agree with Ref. 18 but are different from Ref. 9, in which a FM ground state was predicted.

Smaller formation energies are obtained for the Mn_7Mn_7 configurations. Furthermore, the FM state of the nine configurations is always favored over the AFM state, and $N_{11\bar{3}}$ is the ground state. In this situation, the FM N_{111} state is also lower in energy than the AFM state, which is opposite to the N_{111} Mn_5Mn_5 configuration.

Finally, if we look at the Mn_5Mn_7 configurations, the configuration $N_{\bar{1}\bar{1}\bar{1}}$ with the nearest-neighbor Mn pairs is the ground state with FM ordering, but for the other configura-

TABLE II. The formation energies (E_f), the AFM and FM energy differences (ΔE), the Mn-Mn initial distances (d_{ini}) and relaxed distances (d_{rel}) for FM and AFM states, and the total magnetic moments (M_{tot}) and the atomic magnetic moments (M_1 and M_2) in the Bohr magnetons. In the case of Mn_5Mn_7 , the atomic magnetic moments M_1 and M_2 refer to the substitutional and tetrahedral interstitial atoms.

Configuration		E_f (eV/Mn) (FM)	ΔE (meV/Mn) (AFM-FM)	d_{ini} (Å) (FM,AFM)	d_{rel} (Å) (FM)	d_{rel} (Å) (AFM)	$M_{\text{tot}}(M_1, M_2)$ (FM)	$M_{\text{tot}}(M_1, M_2)$ (AFM)
Mn_5Mn_5	N_{111}	2.320	-472	2.367	2.472	1.832	6.00(2.85, 2.85)	0(1.38, -1.38)
	N_{220}	2.180	51	3.865	3.664	3.453	6.00(2.90, 2.90)	0(2.58, -2.58)
	$N_{11\bar{3}}$	2.332	34	4.532	4.491	4.434	6.00(2.92, 2.92)	0(2.92, -2.92)
	N_{400}	2.237	99	5.466	5.466	5.466	5.98(2.90, 2.90)	0(2.90, -2.90)
	N_{331}	2.229	95	5.956	5.712	5.807	6.00(2.93, 2.93)	0(2.85, -2.85)
	N_{224}	2.336	23	6.694	6.713	6.688	6.00(2.90, 2.90)	0(2.91, -2.91)
	$N_{\bar{3}\bar{3}\bar{3}}$	2.330	16	7.101	7.090	7.091	6.00(2.89, 2.89)	0(2.94, -2.94)
	N_{440}	2.215	16	7.730	7.730	7.730	6.00(2.91, 2.91)	0(2.75, -2.75)
Mn_7Mn_7	N_{444}	2.346	11	9.467	9.467	9.467	6.00(2.90, 2.90)	0(2.94, -2.94)
	N_{111}	1.579	147	2.367	2.494	2.714	6.00(2.53, 2.53)	0(2.37, -2.37)
	N_{220}	1.605	122	3.865	3.688	3.896	6.00(2.55, 2.55)	0(2.25, -2.25)
	$N_{11\bar{3}}$	1.566	19	4.532	4.383	4.331	6.00(2.48, 2.48)	0(2.28, -2.28)
	N_{400}	1.774	374	5.466	5.466	5.466	6.08(2.67, 2.67)	0(2.67, -2.67)
	N_{331}	1.736	43	5.956	5.939	5.997	6.00(2.53, 2.53)	0(2.49, -2.49)
	N_{224}	1.746	32	6.694	6.684	6.686	6.00(2.55, 2.55)	0(2.43, -2.43)
	$N_{\bar{3}\bar{3}\bar{3}}$	1.757	43	7.101	7.168	7.127	6.00(2.47, 2.47)	0(2.42, -2.42)
Mn_5Mn_7	N_{444}	1.774	318	7.730	7.730	7.730	6.00(2.50, 2.50)	0(2.50, -2.50)
	$N_{\bar{1}\bar{1}\bar{1}}$	1.291	159	2.367	2.378	2.317	4.00(1.70, 2.36)	0(2.56, -2.35)
	N_{200}	1.652	-33	2.733	2.604	2.666	4.00(1.05, 2.74)	0(2.83, -2.62)
	$N_{\bar{1}\bar{1}\bar{3}}$	1.953	-20	4.532	4.478	4.400	5.69(2.61, 2.60)	0(2.96, -2.70)
	N_{222}	2.025	24	4.734	4.711	4.754	4.00(0.16, 2.97)	0(3.01, -2.71)
	$N_{\bar{1}\bar{3}\bar{3}}$	2.005	-34	5.956	5.983	5.989	4.00(0.29, 2.93)	0(3.00, -2.68)
	N_{240}	2.025	-54	6.111	6.113	6.099	5.96(2.88, 2.53)	0(3.00, -2.72)
	N_{333}	2.056	-9	7.101	7.104	7.102	6.21(2.88, 2.66)	0(2.99, -2.68)
N_{244}	2.031	-40	8.199	8.199	8.195	6.02(2.88, 2.55)	0(3.02, -2.67)	

tions, the AFM state is lower in energy than the FM state, except for N_{222} . Summarizing the formation energies for all configurations for the three situations, the FM state of configuration $\text{Mn}_5\text{Mn}_7 N_{\bar{1}\bar{1}\bar{1}}$ is the ground state. This shows that the interstitial site of the Mn dopant helps us to stabilize the nearest neighbor substitutional site to realize the FM state. This result is consistent with the prediction in Ref. 9. Furthermore, the energy difference between the FM and AFM states for this configuration is 159 meV and is higher than that for Ge doped by Mn.^{6,18} This indicates that a higher Curie temperature may be obtained for Si doped with Mn, but the disadvantage is that the magnetic moment per Mn atom decreases from $3\mu_B$ to $2\mu_B$.

We also calculated the FM and AFM orderings for the other TM dopants for all configurations. The results for the ground states are summarized in Table III. We find that all the TM atoms tend to cluster as the ground states are always the $X_S X_T N_{\bar{1}\bar{1}\bar{1}}$ configurations, except for Si doped with Ni, whose ground state is the $N_{11\bar{3}} X_T X_T$ configuration. As we saw in Sec. IV, the total magnetic moment for a single TM atom at a substitutional position in Si differs from the total magnetic moment for an interstitial position. This opens up

the possibility of the existence of ferrimagnetic states in which the different moments of the TM atoms are opposite, while a spontaneous magnetization remains. This is indeed the case for Si doped with Cr: this system is not ferromagnetic but ferrimagnetic and has a nonzero total magnetic moment of $2\mu_B$. For the other TM atoms, i.e., V, Co, and Ni, we find that their ground state configurations are nonmagnetic,

TABLE III. The formation energies (E_f), the configurations, the X - X initial distances (d_{ini}) and relaxed distances (d_{rel}), the total magnetic moments (M_{tot}), and atomic magnetic moments (M_1 and M_2) in the Bohr magnetons for the ground state of Si doped by V, Cr, Fe, Co, and Ni. The units are the same as those in Table II.

TM	Configuration	E_f	d_{ini}	d_{rel}	$M_{\text{tot}}(M_1, M_2)$
V	$N_{\bar{1}\bar{1}\bar{1}}/X_S X_T$	1.326	2.367	2.220	0.00(0.00, 0.00)
Cr	$N_{\bar{1}\bar{1}\bar{1}}/X_S X_T$	1.704	2.367	2.099	2.00(-0.20, 1.64)
Fe	$N_{\bar{1}\bar{1}\bar{1}}/X_S X_T$	1.296	2.367	2.377	3.38(1.20, 1.98)
Co	$N_{\bar{1}\bar{1}\bar{1}}/X_S X_T$	0.941	2.367	2.473	0.00(0.00, 0.00)
Ni	$N_{11\bar{3}}/X_T X_T$	0.718	4.532	3.980	0.00(0.00, 0.00)

even if we start our relaxation procedure from an initial FM configuration. For Fe, the ground state is found to be FM.

VII. CONCLUSIONS

By using first-principles techniques, we studied the formation energy and magnetization of six TM impurities (V, Cr, Mn, Fe, Co, and Ni) in Si, but first, the level filling mechanism and the saturation of the magnetization of the TM-alloy were investigated in the zinc-blende structure. We considered three different positions for the impurity in the Si crystal: the tetrahedrally oriented interstitial position, the hexagonally oriented interstitial position, and the substitutional position. We showed that all impurities prefer an interstitial position, which is in contrast to doping of Ge with transition metal impurities. Besides the most often used doping with Mn, it is shown that V and Cr also have large magnetic moments. As interstitial doping can easily lead to clustering of the impurities, and consequently, a decrease in total magnetic moment, it is important to try to stabilize the substitutional dopants. We showed that this can be realized for Mn, Fe, Co, and Ni in Si by applying a positive pressure (but of these impurities, only Mn realizes a total magnetic

moment larger than $1\mu_B$). This suggests that a spintronic material based on Si may be more easily realized if strain fields are present. However, applying a pressure also decreases the total magnetic moment. Finally, we investigated the clustering of the TM impurities in Si and their FM and AFM orderings by considering two TM atoms doped into Si for different distances between them. For most TMs, the nearest-neighbor TM pair, in which one is at the substitutional site and the other is at the tetrahedral interstitial site, has the lowest formation energy. Among those TMs, the Mn and Fe pairs show ferromagnetism, while V, Co, and Ni pairs are nonmagnetic. Interestingly, ferrimagnetic behavior is found for the Cr pair. To conclude, we may say that the best candidates to realize a magnetic semiconductor based on Si are Mn and Cr dopants.

ACKNOWLEDGMENTS

All the calculations were performed in the Computer Network Information Center, Chinese Academy of Sciences and on CalcUA at UA. This work is supported by NSFC Grant No. 62525405 and the Knowledge Innovation Project of CAS, and also by the Flemish Science Foundation (FWO-VI) and the Flemish-Chinese bilateral project.

*zzzhong@semi.ac.cn

†bart.partoens@ua.ac.be

‡kchang@semi.ac.cn

§francois.peeters@ua.ac.be

¹S. A. Wolf, D. D. Awschalom, R. A. Buhman, J. M. Daughton, S. von Molár, M. L. Roukes, A. Y. Chtchelkanova, and D. M. Treger, *Science* **294**, 1488 (2001).

²S. A. Wolf, A. Y. Chtchelkanova, and D. M. Treger, *IBM J. Res. Dev.* **50**, 101 (2006).

³A. M. Nazmul, T. Amemiya, Y. Shuto, S. Sugahara, and M. Tanaka, *Phys. Rev. Lett.* **95**, 017201 (2005).

⁴S. J. Pearton, C. R. Abernathy, M. E. Overberg, G. T. Thaler, D. P. Norton, N. Theodoropoulou, A. F. Hebard, and Y. D. Park, *J. Appl. Phys.* **93**, 1 (2003).

⁵Y. D. Park, A. T. Hanbicki, S. Erwin, C. Hellberg, J. Sullivan, J. Mattson, T. F. Ambrose, A. Wilson, G. Spanos, and B. Jonker, *Science* **295**, 651 (2002); S. Cho, S. Choi, S. C. Hong, Y. Kim, J. B. Ketterson, B. J. Kim, Y. C. Kim, and J. H. Jung, *Phys. Rev. B* **66**, 033303 (2002); O. Kazakova, J. S. Kulkarni, J. D. Holmes, and S. O. Demokritov, *ibid.* **72**, 094415 (2005).

⁶Y. J. Zhao, T. Shishidou, and A. J. Freeman, *Phys. Rev. Lett.* **90**, 047204 (2003).

⁷A. Continenza, G. Profeta, and S. Picozzi, *Phys. Rev. B* **73**, 035212 (2006).

⁸M. Bolduc, C. Awo-Affouda, A. Stollenwerk, M. B. Huang, F. G. Ramos, G. Agnello, and V. P. LaBella, *Phys. Rev. B* **71**, 033302 (2005).

⁹F. Bernardini, S. Picozzi, and A. Continenza, *Appl. Phys. Lett.* **84**, 2289 (2004).

¹⁰G. M. Dalpian, A. J. R. da Silva, and A. Fazzio, *Phys. Rev. B* **68**, 113310 (2003).

¹¹A. J. R. da Silva, A. Fazzio, and A. Antonelli, *Phys. Rev. B* **70**, 193205 (2004).

¹²M. C. Qian, C. Y. Fong, K. Liu, W. E. Pickett, J. E. Pask, and L. H. Yang, *Phys. Rev. Lett.* **96**, 027211 (2006).

¹³H. Wu, P. Kratzer, and M. Scheffler, *Phys. Rev. Lett.* **98**, 117202 (2007).

¹⁴P. R. Bandaru, J. Park, J. S. Lee, Y. J. Tang, L. H. Chen, S. Jin, S. A. Song, and J. R. O'Brien, *Appl. Phys. Lett.* **89**, 112502 (2006).

¹⁵C. Awo-Affouda, M. Bolduc, M. B. Huang, F. Ramos, K. A. Dunn, B. Thiel, G. Agnello, and V. P. LaBella, *J. Vac. Sci. Technol. A* **24**, 1644 (2006).

¹⁶H. Katayama-Yoshida and A. Zunger, *Phys. Rev. B* **31**, 8317 (1985).

¹⁷F. Beeler, O. K. Andersen, and M. Scheffler, *Phys. Rev. B* **41**, 1603 (1990).

¹⁸H. Weng and J. Dong, *Phys. Rev. B* **71**, 035201 (2005).

¹⁹Y. Kamon, H. Harima, A. Yanase, and H. Katayama-Yoshida, *Physica B* **308-310**, 391 (2001).

²⁰G. Kresse and J. Furthmüller, *Comput. Mater. Sci.* **6**, 15 (1996).

²¹P. E. Blöchl, *Phys. Rev. B* **50**, 17953 (1994).

²²J. P. Perdew, J. A. Chevary, S. H. Vosko, K. A. Jackson, M. R. Pederson, D. J. Singh, and C. Fiolhais, *Phys. Rev. B* **46**, 6671 (1992).

²³B. Roessli, P. Boni, W. E. Fischer, and Y. Endoh, *Phys. Rev. Lett.* **88**, 237204 (2002).

²⁴O. Schob and E. Parthé, *Acta Crystallogr.* **17**, 452 (1964).

²⁵E. G. Moroni, W. Wolf, J. Hafner, and R. Podloucky, *Phys. Rev. B* **59**, 12860 (1999); T. Jeong and W. E. Pickett, *ibid.* **70**, 075114 (2004).

²⁶Y. Ishikawa, G. Shirane, J. A. Tarvin, and M. Kohgi, *Phys. Rev. B* **16**, 4956 (1977).